

## Experimental Investigation of the Role of Fluid Turbulent Stresses and Edge Plasma Flows for Intrinsic Rotation Generation in DIII-D *H*-Mode Plasmas

S. H. Müller,<sup>1,2</sup> J. A. Boedo,<sup>1</sup> K. H. Burrell,<sup>3</sup> J. S. deGrassie,<sup>3</sup> R. A. Moyer,<sup>1</sup> D. L. Rudakov,<sup>1</sup> and W. M. Solomon<sup>4</sup>

<sup>1</sup>Center for Energy Research, University of California of San Diego, 9500 Gilman Drive, M/C 0417, La Jolla, California 92093, USA

<sup>2</sup>Center for Momentum Transport and Flow Organization

<sup>3</sup>General Atomics, P.O. Box 85608, San Diego, California 92186-5608, USA

<sup>4</sup>Princeton Plasma Physics Laboratory, P.O. Box 451, Princeton, New Jersey 08543-0451, USA

(Received 24 November 2010; published 15 March 2011)

The first measurements of turbulent stresses and flows inside the separatrix of a tokamak *H*-mode plasma are reported, using a reciprocating multitip Langmuir probe at the DIII-D tokamak. A strong co-current rotation layer at the separatrix is found to precede intrinsic rotation development in the core. The measured fluid turbulent stresses transport toroidal momentum outward against the velocity gradient and thus try to sustain the edge layer. However, large kinetic stresses must exist to explain the net inward momentum transport leading to co-current core plasma rotation. The importance of such kinetic stresses is corroborated by the success of a simple orbit loss model, representing a purely kinetic mechanism, in the prediction of features of the edge corotation layer.

DOI: 10.1103/PhysRevLett.106.115001

PACS numbers: 52.35.Ra, 52.25.Fi, 52.55.Dy, 52.55.Fa

Toroidal plasma rotation has a wide range of beneficial effects on stability, confinement, and performance in tokamaks [1]. In addition to the driven rotation by tangential neutral beam injection (NBI), tokamak plasmas also exhibit rotation in the case of no apparent external momentum sources, which is referred to as *intrinsic* rotation. Because of both the practical relevance for magnetic confinement fusion and the broad general physics interest in systems that are apparently able to spontaneously change their rotation properties, intrinsic rotation has been extensively studied experimentally [2–8] and theoretically [9,10]. Experiments have inferred an “intrinsic torque” located at the plasma edge [8,11], and a role of scrape-off layer flows as a source for toroidal rotation has been suggested [4]. Nondiffusive nonconvective turbulent stresses (dubbed *residual stresses*) are strong candidates to explain the spin-up of the core plasma [9].

In this Letter, we report the first measurements of turbulent stresses and flows inside the last closed flux surface (separatrix) of a tokamak plasma in high-confinement mode (*H* mode). The observation of a strong edge co-current rotation layer [4,11] is found to precede the development of intrinsic core rotation. The measured fluid turbulent stresses transport momentum outward and thus try to sustain the edge layer, but strong kinetic stresses are required to explain the net inward transport of toroidal momentum from the layer into the core. Such strong kinetic stresses cannot be obtained within the established theory of (weakly) nonuniform fluids of Chapman and Enskog [12] and its application to magnetized plasmas by Braginskii [13], which break down in an *H*-mode pedestal since the macroscopic gradient scale lengths are of the order of the ion Larmor radius.

Recall the toroidal angular momentum balance equation for a magnetic field  $\mathbf{B} = R^{-1}(I\hat{\varphi} + \hat{\varphi} \times \nabla\Psi) + \mathbf{B}^{\text{na}}$  ( $R$  is

the distance to the major axis,  $\hat{\varphi}$  is the toroidal unit vector,  $-2\pi\Psi \equiv \int d^2\sigma \cdot \mathbf{B}$  is the poloidal flux):

$$\begin{aligned} \partial_t(mR\Gamma_\varphi) + \nabla \cdot (R\Pi \cdot \hat{\varphi}) - q(n\partial_t + \Gamma \cdot \nabla)\Psi \\ - qR(nE_\varphi^{\text{na}} + \hat{\varphi} \cdot \Gamma \times \mathbf{B}^{\text{na}}) = R(C_\varphi + S_\varphi), \end{aligned} \quad (1)$$

where  $n \equiv \int d^3u f$ ,  $\Gamma_i \equiv nv_i \equiv \int d^3u u_i f$ ,  $\Pi_{ij} \equiv m \int d^3u u_i u_j f$ ,  $C_\varphi \equiv m \int d^3u u_\varphi \mathcal{C}$ , and  $S_\varphi \equiv m \int d^3u u_\varphi \mathcal{S}$  are the moments of distribution function  $f$ , collision operator  $\mathcal{C}$  and kinetic source  $\mathcal{S}$  ( $u_i$  are the velocity space coordinates). The first three terms of Eq. (1) correspond to conservation of canonical angular momentum  $mRu_\varphi - q\Psi$  in phase space. In the absence of nonaxisymmetric fields  $E_\varphi^{\text{na}} = 0$ ,  $\mathbf{B}^{\text{na}} = 0$ , explicit sources  $S_\varphi = 0$ , in an equilibrium characterized by  $\partial_t\Psi = 0$  and  $\Gamma_\rho = 0$  ( $\hat{\rho} \equiv \nabla\Psi/|\nabla\Psi|$ ), and noting that  $C_\varphi \propto -v_\varphi$  always opposes rotation, the only remaining candidate to explain an increase of ion angular momentum in a volume  $V(\psi)$  is a finite stress at the boundary  $\oint_{\partial V(\psi)} d^2\sigma R\Pi_{\varphi\rho} \neq 0$ . The total stress can be written as  $\Pi_{\varphi\rho} = mnv_\varphi v_\rho + \pi_{\varphi\rho}$ , where  $\pi_{\varphi\rho}$  represents kinetic stresses that cannot be expressed as functions of lower-order moments of  $f$ . Chapman-Enskog closure theory approximates  $\pi_{ij}$  in terms of the rate-of-strain tensor  $W_{ij} \equiv \partial_i v_j + \partial_j v_i - \frac{2}{3}\partial_k v_k \delta_{ij}$ , assuming a first-order expansion of  $f$  about a Maxwellian [12,13]. Inherently, the estimates of  $\pi_{\varphi\rho}$  are small, so that studies have focused on the  $mnv_\varphi v_\rho$  term [2,9]. It is common to decompose all variables in time-average and fluctuating quantities, e.g.,  $A = \langle A \rangle + \tilde{A}$ , and writing

$$\langle nv_\varphi v_\rho \rangle = \langle n \rangle \langle \tilde{v}_\varphi \tilde{v}_\rho \rangle + \langle v_\varphi \rangle \langle \tilde{n} \tilde{v}_\rho \rangle + \langle \tilde{n} \tilde{v}_\varphi \tilde{v}_\rho \rangle, \quad (2)$$

where  $\langle v_\rho \rangle = 0$  is assumed and  $\langle n \rangle \langle \tilde{v}_\varphi \tilde{v}_\rho \rangle$ ,  $\langle v_\varphi \rangle \langle \tilde{n} \tilde{v}_\rho \rangle$ , and  $\langle \tilde{n} \tilde{v}_\varphi \tilde{v}_\rho \rangle$  are the contributions from Reynolds stress, particle transport, and triple correlations, respectively.

In this Letter, using a reciprocating multitip Langmuir probe [11,14], we present the first direct measurements of the terms in Eq. (2) in a tokamak  $H$ -mode pedestal. We use an arrangement of five probe tips (size 2 mm) [2] in the form of a tilted cross (distance between opposing tips 1 cm; tilt angle 30 degrees). Two pins, separated by a barrier (height 3 mm), are aligned along  $\hat{\varphi}$  and measure the (mostly  $D^+$ ) ion saturation fluxes  $\Gamma_\pm$  (bias  $-300$  V). A theory of ion collection by absorbing objects in combined parallel and perpendicular flows [15] is used to calculate the flow velocity in the direction of tip alignment and the unperturbed density:  $v_\varphi = \frac{1}{2}c_s \ln(\Gamma_-/\Gamma_+)$ ;  $n = [\exp(1)/c_s] \sqrt{\Gamma_- \Gamma_+}$ . Note that the sound speed  $c_s \equiv \sqrt{(T_e + T_i)/m_i} \approx \sqrt{2T_e/m_i}$  cancels in  $nv_\varphi$ . To compare  $\langle n \rangle$  and  $\langle v_\varphi \rangle$  against other diagnostics,  $\langle T_e \rangle$  is measured on the central tip using a harmonics technique [16]. The two remaining, poloidally separated tips measure the floating potential difference  $\delta V$ , from which  $\tilde{E}_\theta \approx -\delta V/\delta \ell$  and  $\tilde{v}_\rho \approx -\tilde{E}_\theta/B_\varphi$  are obtained, where  $\hat{\theta} \equiv \hat{\rho} \times \hat{\varphi}$  and  $\delta \ell$  is the poloidal separation. We use a sliding median filter of 0.5 ms width, corresponding to 1 mm of probe motion, to perform the background subtraction and a 2 ms sliding mean to calculate averages. Halving or doubling these choices does not significantly change the results. The results from all diagnostics, including the probe, which is situated 18.8 cm below the midplane, were mapped to  $\psi$  using the EFIT equilibrium reconstruction code, resulting in good agreement between the probe and the Thomson scattering diagnostic for the  $n$  and  $T_e$  profiles. The probe does not perturb the discharge measurably by other diagnostics.

The reported experiment made use of the capability of DIII-D to produce edge localized mode (ELM)-free  $H$ -mode plasmas interchangeably with electron cyclotron heating (ECH) and co- and counter-current NBI, thereby altering the torque input while keeping the power input constant at about 1 MW. The ITER-like lower-single-null shape and base parameters of  $B_{\varphi 0} = -1.6$  T,  $I_p = 1.3$  MA, and  $n_0 = 3 \times 10^{19} \text{ m}^{-3}$  were optimized for a reliable transition from low- to high-confinement mode ( $L$ - $H$  transition) at the lowest possible powers and extremely long ELM-free characteristics [Fig. 1]. All three heating schemes, turned on at 1500 ms, produced an  $L$ - $H$  transition reliably at  $1575 \pm 25$  ms, resulting in a prompt increase of the peaked core  $T_e$  profile and a slow, approximately linear increase of the flat core density profile. Beam fuelling plays a negligible role in this density rise [Fig. 1]. The probe plunges were timed to reach the dwell point, on a shot-to-shot basis, at 1650, 1900, and 2200 ms (NBI: 2300 ms). An earlier plunge was usually performed at 1000 ms for Ohmic and  $L$ -mode data. Approximately

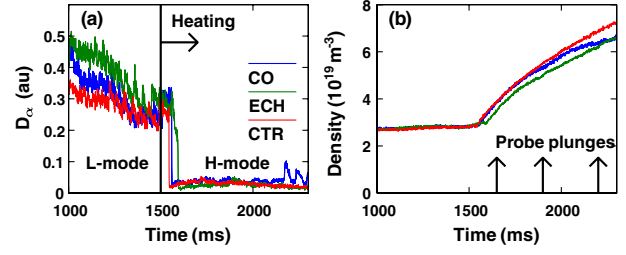


FIG. 1 (color online). (a)  $D_\alpha$  signal as an indicator for  $L$ - $H$  transition and ELM freeness. (b) Line-integrated density evolution. The three probe plunges at different delays were performed in identical repeat shots and immediately followed by beam blips for a snapshot of the  $C^{6+}$  rotation profile.

unperturbative diagnostic beam blips of 2 ms length were fired immediately after the dwell time to obtain snapshot profiles of the  $C^{6+}$  rotation. The main data set thus consists of a  $3 \times 3$  matrix of different torques and delays in early ELM-free  $H$  mode. Against our expectations, the  $n$  and  $T_e$  profiles in the lower half of the pedestal, which is accessible to the probe, were found *identical* for all nine cases. With the gradients frozen, the pedestal height and width increase as the density rises.

Figure 2 shows the combined  $C^{6+}$  and  $D^+$  rotation profiles, where we note that the impurity rotation is a good approximation for the main ion rotation in the core where gradients are weak, but not necessarily in the edge region [11]. The probe data shows clear evidence of a robust co-current rotation layer at the plasma edge. The layer is only 1 cm wide, peaks just inside the EFIT separatrix, and rotates co-current even when counter torque is applied to the core, although its magnitude decreases from 35 km/s to 25 km/s in this case. By the time of the earliest probe plunge 50 ms after the  $L$ - $H$  transition, the layer has developed to its full size from a rudimentary feature in the Ohmic plasma 650 ms earlier. The lack of evolution over the following 650 ms in  $H$  mode suggests that the  $L$ - $H$  transition is the defining event for the rapid formation of the layer in our conditions. However, equally strong layers have been observed in different steady-state  $L$  modes [11], indicating more complex conditions for layer formation.

In the ECH case with zero applied torque [Figs. 2(b) and 2(e)], intrinsic core rotation develops over a period of 600 ms after the first observation of the edge layer. The latest rotation measurement, peaking at 40 km/s, coincides in magnitude with the edge layer, but a dip in the rotation profile disproves a simple picture in which the core responds to a rotating boundary via viscous diffusion. A specific reanalysis of main-ion rotation data in similar helium plasmas [6], motivated by the Mach probe measurements, confirms both the existence of the edge corotation layer and the persistence of the dip during intrinsic rotation development. The application of co- and counter-current NBI drive [Figs. 2(a) and 2(d) and Figs. 2(c) and 2(f)] has a strong impact on the velocity profile and its

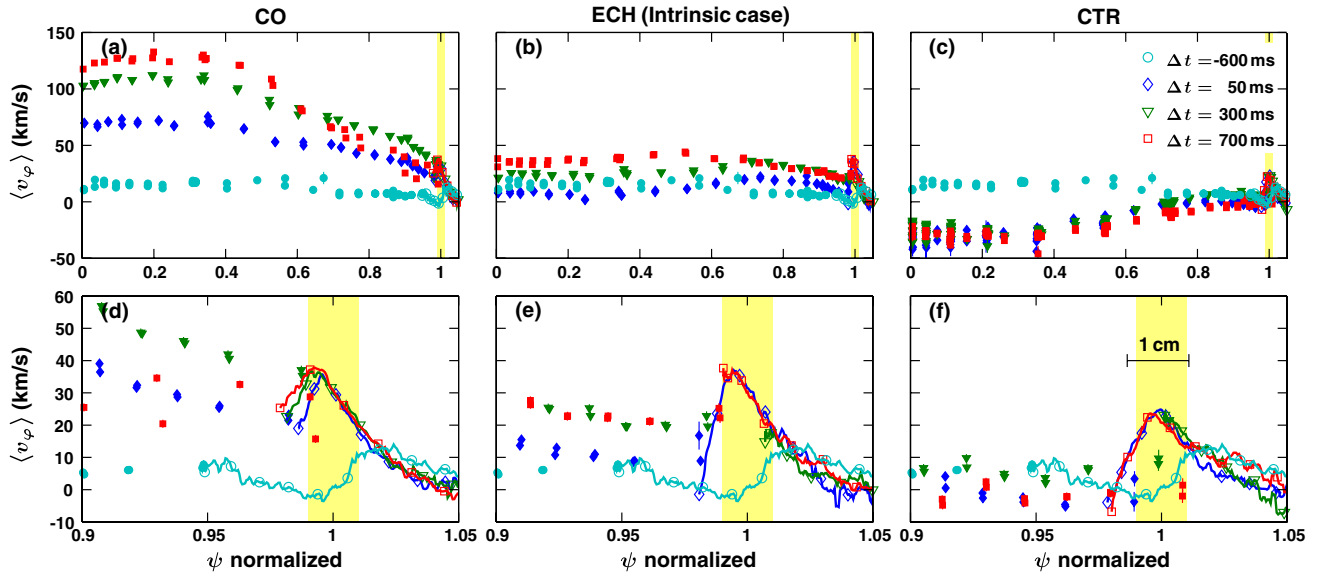


FIG. 2 (color online). (a)–(c) Combined  $C^{6+}$  (filled symbols) and probe (lines with open symbols) rotation profiles for different torque inputs and delays  $\Delta t$  after the  $L$ - $H$  transition. An Ohmic profile is shown at  $\Delta t = -600$  ms. Shaded areas indicate an estimated 95% confidence interval for the separatrix position. (d)–(f) Expanded view of the edge region. Error estimates are discussed in Fig. 4.

gradient, but the total resulting rotation appears well described as the sum of a constant intrinsic part plus the beam-driven part, underlining the nondiffusive and non-convective nature of the stresses leading to intrinsic rotation.

The measured turbulence is broadband, ranging from 1 kHz to 1 MHz, with autocorrelation times of 2 – 20  $\mu$ s. The normalized fluctuation levels are low:  $\langle \tilde{n}^2 \rangle^{1/2} / \langle n \rangle \sim \langle \delta \tilde{v}^2 \rangle^{1/2} / \langle T_e / e \rangle \sim \langle \tilde{v}_\varphi^2 \rangle^{1/2} / \langle c_s \rangle \sim 5\%$  for  $\psi \lesssim 1$ , increasing to about 30% at  $\psi \approx 1.03$ . Absolute fluctuation levels and autocorrelation times exhibit a minimum at the peak of the edge corotation layer.

Figure 3 shows the toroidal momentum density  $\langle n v_\varphi \rangle$  (a),(b) of the edge layer and the measurements of the momentum transport terms in Eq. (2),  $\langle n \rangle \langle \tilde{v}_\varphi \tilde{v}_\rho \rangle$  (c),(d) and  $\langle v_\varphi \rangle \langle \tilde{n} \tilde{v}_\rho \rangle$  (e),(f) for the co-current NBI and ECH cases. The contribution of triple correlations  $\langle \tilde{n} \tilde{v}_\varphi \tilde{v}_\rho \rangle$  was generally found negligible. The particle transport contribution [Figs. 3(e) and 3(f)] becomes negative inside the peak of the layer, which is consistent with the global density rise [Fig. 1].

The Reynolds stress term  $\langle n \rangle \langle \tilde{v}_\varphi \tilde{v}_\rho \rangle$  [Figs. 3(c) and 3(d)] is effectively zero outside the layer's peak and becomes increasingly positive further inward, dominating over the inward-directed term  $\langle v_\varphi \rangle \langle \tilde{n} \tilde{v}_\rho \rangle$  in magnitude. It is neither proportional to  $-\langle v_\varphi \rangle$  nor to  $-\partial_\rho \langle v_\varphi \rangle$  and thus satisfies the definition of a *residual stress*, which acts to transport (positive) momentum outward, up the layer's inner flank, thus trying to sustain the corotation layer. However, this exerts a countercurrent torque onto the core, which is clearly inconsistent with the fact that we see the core spinning up in the *co-current* direction.

Since the measured fluid turbulent stresses do not lead to a globally consistent picture, we revisit the possibility of kinetic stresses in the edge and estimate the required magnitudes from a global torque balance. Figure 4(a) shows the rate of change of cumulative angular momentum  $L_\varphi(\psi) \equiv \int_{V(\psi)} d^3x m R n v_\varphi$ , estimated from Thomson

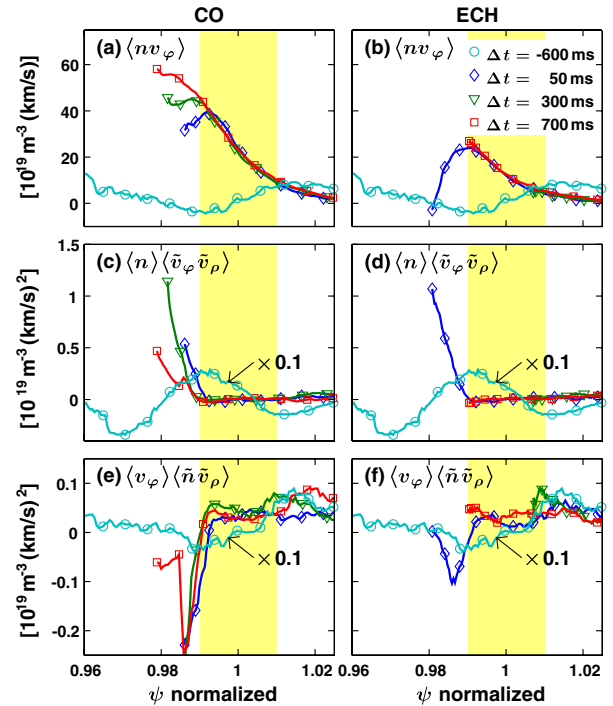


FIG. 3 (color online). Probe measurements of fluid turbulent stresses.

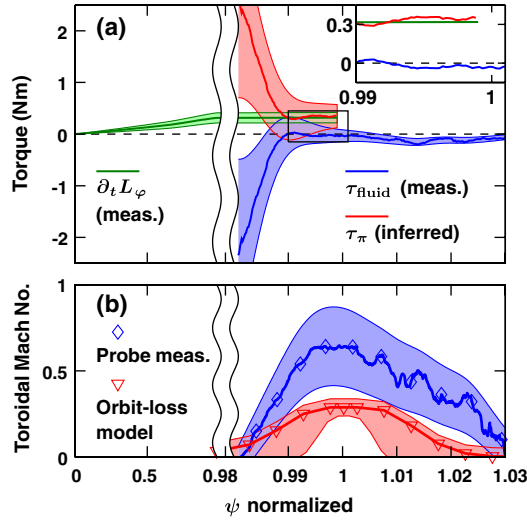


FIG. 4 (color online). (a) Torque balance for the ECH  $H$ -mode case at  $\Delta t = 50$  ms. (b) A simple orbit loss model correctly predicts direction, location and width of the edge corotation layer. Shaded areas represent estimated 95% confidence intervals.

scattering and charge-exchange-recombination spectroscopy. Under the present assumptions, this must be locally equal to the torque  $\tau_{\Pi}(\psi) \equiv -\oint_{\partial V(\psi)} d^2\sigma R \langle \Pi_{\varphi\rho} \rangle$ . The contribution from the measured fluid stresses,  $\tau_{\text{fluid}} \equiv -\oint_{\partial V(\psi)} d^2\sigma R m \langle n v_{\varphi} v_{\rho} \rangle = -2\pi m L_{\text{eff}} R^2 \langle n v_{\varphi} v_{\rho} \rangle$ , is also shown. Here, we assumed that the measurements are representative for an effective poloidal length of  $L_{\text{eff}} \sim 2$  m on the low-field side and neglected contributions from the high-field side. Since  $R^2 \langle n v_{\varphi} v_{\rho} \rangle$  is most likely not a flux function, this assumption is subject to large uncertainties, which are factored into the error estimates in Fig. 4. For  $\psi \approx 0.98$ ,  $\tau_{\text{fluid}}$  contributes  $-2$  Nm of torque, which is opposite and much larger than the necessary  $+0.3$  Nm that the core spin-up requires. It is thus necessary to infer a large torque  $\tau_{\pi} \approx +2.3$  Nm from the kinetic stresses  $\langle \pi_{\varphi\rho} \rangle$ , about 20 times larger than what Chapman-Enskog theory would provide. For  $\psi \sim 1$  at the layer's peak where the gradient is zero,  $\tau_{\text{fluid}} \approx 0$  is measured [Fig. 4, inset], such that  $\tau_{\pi}$  has to account for the full  $+0.3$  Nm of torque. Taken together with the constraints from the rotation-profile evolution discussed earlier in Fig. 2, we must therefore require that the kinetic stresses  $\langle \pi_{\varphi\rho} \rangle$  have the *same nondiffusive nonconvective characteristics as a residual stress* everywhere in the interval  $0.98 \leq \psi \leq 1$ .

To give an example of a process that would lead to such kinetic stresses, results from a simple orbit loss model [7] are shown in Fig. 4(b). Conservation of canonical angular momentum along particle trajectories requires that comoving ions drift inward, while countermoving ones drift outward. In the vicinity of  $\psi = 1$ , this mechanism leads to a loss cone in velocity space, which alters the moments of  $f$ , including  $v_{\varphi}$  and  $\Pi_{\varphi\rho}$ . The model correctly predicts the

existence, direction, position, and width of the edge corotation layer, while underestimating its magnitude by a factor of 2. This highlights the necessity to include purely kinetic processes in the search for residual stresses in a tokamak  $H$ -mode pedestal and develop appropriate theory. Our results indicate that the decomposition  $\Pi_{\varphi\rho} = m n v_{\varphi} v_{\rho} + \pi_{\varphi\rho}$  poorly reflects the nature of the present physical processes, suggesting the exploration of other venues.

In summary, we have presented the first measurements of fluid turbulent stresses and flows in a tokamak  $H$ -mode pedestal. The core rotation was observed to respond to the emergence of a strong edge co-current rotation layer, which appears to be at least partially created by purely kinetic processes. Full- $f$  gyrokinetic codes that can treat the plasma edge [17] should be in a position to observe an edge corotation layer and confirm the existence of kinetic stresses that greatly surpass the Chapman-Enskog estimates in an  $H$ -mode pedestal. The smaller intrinsic rotation in  $L$  mode in DIII-D could potentially be explained by an increased interaction of ion orbits with turbulence, leading to a symmetrization of the loss cone. The observed countercurrent intrinsic rotation in  $L$  mode in other devices [4,5] may be related to other effects.

This work was supported by the U.S. Department of Energy under DE-FG02-07ER54917 and DE-FC02-04ER54698. Many valuable contributions from P. H. Diamond, P. Gohil, I. H. Hutchinson, H. Reimerdes, G. R. Tynan, and J. G. Watkins are gratefully acknowledged.

- [1] K. H. Burrell, *Phys. Plasmas* **4**, 1499 (1997).
- [2] C. Hidalgo *et al.*, *Phys. Rev. Lett.* **91**, 065001 (2003); B. Gonçalves *et al.*, *Phys. Rev. Lett.* **96**, 145001 (2006).
- [3] J. E. Rice *et al.*, *Nucl. Fusion* **45**, 251 (2005); *Plasma Phys. Controlled Fusion* **50**, 124042 (2008).
- [4] B. LaBombard *et al.*, *Phys. Plasmas* **12**, 056111 (2005); *Phys. Plasmas* **15**, 056106 (2008).
- [5] A. Bortolon *et al.*, *Phys. Rev. Lett.* **97**, 235003 (2006); R. A. Pitts *et al.*, *J. Nucl. Mater.* **363–365**, 505 (2007).
- [6] J. S. deGrassie *et al.*, *Phys. Plasmas* **14**, 056115 (2007).
- [7] J. S. deGrassie *et al.*, *Nucl. Fusion* **49**, 085020 (2009).
- [8] W. M. Solomon *et al.*, *Nucl. Fusion* **49**, 085005 (2009).
- [9] Ö. D. Gürçan *et al.*, *Phys. Plasmas* **14**, 042306 (2007); P. H. Diamond *et al.*, *Nucl. Fusion* **49**, 045002 (2009).
- [10] Y. Camenen *et al.*, *Phys. Rev. Lett.* **102**, 125001 (2009).
- [11] J. A. Boedo *et al.*, *Phys. Plasmas* (to be published).
- [12] S. Chapman and T. G. Cowling, *The Mathematical Theory of Non-uniform Gases* (Cambridge University Press, Cambridge, England, 1953).
- [13] S. I. Braginskii, *Reviews of Plasma Physics* edited by M. A. Leontovich (Consultants Bureau, New York, 1965), Vol. 1, p. 205.
- [14] R. A. Moyer *et al.*, *Phys. Plasmas* **2**, 2397 (1995).
- [15] I. H. Hutchinson, *Phys. Plasmas* **15**, 123503 (2008).
- [16] D. L. Rudakov *et al.*, *Rev. Sci. Instrum.* **72**, 453 (2001).
- [17] C. S. Chang *et al.*, *Phys. Plasmas* **11**, 2649 (2004); C. S. Chang and S. Ku, *Phys. Plasmas* **15**, 062510 (2008).